The University of Osaka
Institutional Knowledge Archive

The University of Osaka Institutional Knowledge Archive : OUKA

https://ir.library.osaka-u.ac.jp/

The University of Osaka

Time Dependent Numerical Analysis of Stationary GTA Welding Process †

TANAKA Manabu*, USHIO Masao** and John J. LOWKE***

Abstract

A development of a numerical model of GTA welding process is useful for understanding the heat transfer phenomena in the process and clarifying those effects on the weld penetration geometry. This paper presents results for the stationary argon GTA welding process at the atmospheric pressure. The whole region of the welding process, namely, tungsten cathode, arc plasma and stainless steel anode is treated in a unified numerical model to take into account the close interaction between the arc plasma and the molten anode. The time dependent two-dimensional distributions of temperature and velocity in the whole region of the welding process are predicted at a current of 150 A. The weld penetration geometry as a function of time is thus predicted. It is shown also that calculated convective flow in the weld pool is mainly dominated by the drag force of the cathode jet and the Marangoni force as compared with the other two driving forces, namely, the buoyancy force and the electromagnetic force.

1. Introduction

Electric arcs have been applied to many kinds of industrial materials processing such as welding, cutting, spraying, melting, heating, refining and so on. In the welding process by the electric arcs, it is important to understand the heat transfer phenomena from the arc to the materials and also the heat transport phenomena in the materials, because there is close interaction between the arc plasma and the materials and then weld penetrations will be dominated by the heat transport phenomena through their interaction[1]. The plasma state of the arc, namely, temperature distribution, fluid flow velocity, arc current density and so on in the arc plasma strongly affects the heat transfer into the materials[2]. The heat transport phenomena in the materials practically consist of heat conduction and heat convection owing to the liquid flow in the weld pool. The driving forces of this convective flow in the weld pool are also based on the close interaction between the arc plasma and the weld pool[3].

The present paper is focused on a numerical study of a gas tungsten arc (GTA) welding process. We use a unified numerical model of stationary argon GTA welding process. The whole region of the welding process, namely, tungsten cathode, arc plasma and stainless steel anode is treated in the unified numerical model to take into account the close interaction between the arc plasma and the molten anode. The basic model and procedure is that of our previous paper[4], but extended to include time dependent calculation. We give the predicted profile of weld penetration as a function of time.

2. A Unified Numerical Model

The tungsten cathode, arc plasma and anode are described relative to a cylindrical coordinate, assuming rotational symmetry around the arc axis. The calculation domain is the same as in the previous paper[4]. The flow is
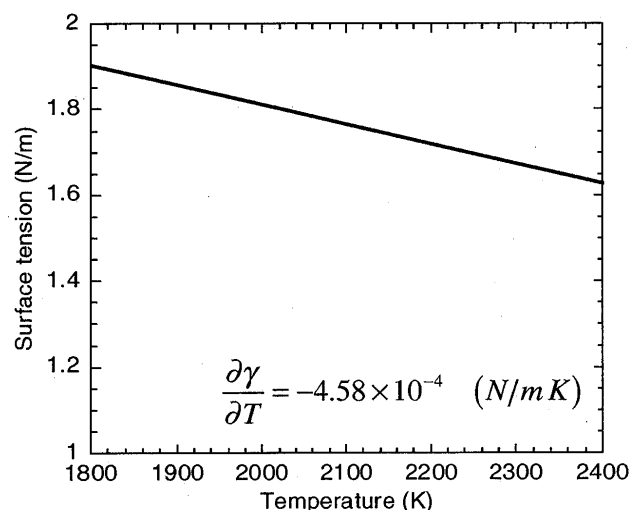

Fig. 1 Assumption of surface tension of molten SUS304.

$$\frac{\partial \gamma}{\partial T} = -4.58 \times 10^{-4} \quad (N/mK)$$

assumed to be laminar, the electron and heavy particle temperatures are assumed to be equal and the effects of the non-collisional space-charged zone in front of both electrodes are neglected. Furthermore, the anode surface is assumed to be flat and unperturbed by the arc pressure. The anode is a stainless steel, SUS304, and its melting point is assumed to be 1750 K with a constant temperature coefficient of surface tension as shown in **Fig. 1**. The diameter of the tungsten cathode is 3.2 mm with a 60 degrees conical tip. The atmospheric shielding gas of the GTA is assumed to be pure argon.

The governing equations, boundary conditions and numerical method are extended to the time dependent model including the convective effects of the molten anode, compared with those of the previous paper[4], and so only the most pertinent details are outlined here.

The mass continuity equation is

$$\frac{\partial \rho}{\partial t} + \frac{1}{r}\frac{\partial}{\partial r}(r\rho v_r) + \frac{\partial}{\partial z}(\rho v_z) = 0 \qquad (1)$$

The radial momentum conservation equation is

$$\frac{\partial \rho v_r}{\partial t} + \frac{1}{r}\frac{\partial}{\partial r}(r\rho v_r^2) + \frac{\partial}{\partial z}(\rho v_z v_r) = -\frac{\partial P}{\partial r} - j_z B_\theta$$

$$+ \frac{1}{r}\frac{\partial}{\partial r}\left(2r\eta\frac{\partial v_r}{\partial r}\right) + \frac{\partial}{\partial z}\left(\eta\frac{\partial v_r}{\partial z} + \eta\frac{\partial v_z}{\partial r}\right) - 2\eta\frac{v_r}{r^2} \qquad (2)$$

The axial momentum conservation equation is

$$\frac{\partial \rho v_z}{\partial t} + \frac{1}{r}\frac{\partial}{\partial r}(r\rho v_r v_z) + \frac{\partial}{\partial z}(\rho v_z^2) = -\frac{\partial P}{\partial z} + j_r B_\theta$$

$$+ \frac{\partial}{\partial z}\left(2\eta\frac{\partial v_z}{\partial z}\right) + \frac{1}{r}\frac{\partial}{\partial r}\left(r\eta\frac{\partial v_r}{\partial z} + r\eta\frac{\partial v_z}{\partial r}\right) + \rho g \qquad (3)$$

The energy conservation equation is

$$\frac{\partial \rho h}{\partial t} + \frac{1}{r}\frac{\partial}{\partial r}(r\rho v_r h) + \frac{\partial}{\partial z}(\rho v_z h) = \frac{1}{r}\frac{\partial}{\partial r}\left(\frac{r\kappa}{c_p}\frac{\partial h}{\partial r}\right)$$

$$+ \frac{\partial}{\partial z}\left(\frac{\kappa}{c_p}\frac{\partial h}{\partial z}\right) + j_r E_r + j_z E_z - U \qquad (4)$$

The current continuity equation is

$$\frac{1}{r}\frac{\partial}{\partial r}(r j_r) + \frac{\partial}{\partial z}(j_z) = 0 \qquad (5)$$

where t is time, h is enthalpy, P is pressure, v_z and v_r are the axial and radial velocities, j_z and j_r are the axial and radial components of the current density, g is the accelera-

tion due to gravity, κ is the thermal conductivity, c_p is the specific heat, ρ is the density, η is the viscosity, U is the radiation emission coefficient, E_r and E_z are respectively the radial and axial components of the electric field defined by $E_r = -\partial V/\partial r$ and $E_z = -\partial V/\partial z$, where V is electric potential. Instead of the usual representation of the current density as dependent only on the electric field by Ohm's law ($j = \sigma E$, where σ is the electrical conductivity), we also include a term to account for diffusion current from electrons. This term overcomes the problem that the equilibrium electrical conductivity is effectively zero in the plasma close to the electrodes owing to the low plasma temperature. This diffusion term is also consistent with our previous paper, which suggested that the diffusion current would dominate the arc current in the anode boundary layer[5]. Thus,

$$j_r = -\sigma\frac{\partial V}{\partial r} + eD_e\frac{\partial n_e}{\partial r} \qquad (6)$$

and

$$j_z = -\sigma\frac{\partial V}{\partial z} + eD_e\frac{\partial n_e}{\partial z} \qquad (7)$$

where D_e is the electron diffusion coefficient, e is the elementary charge and n_e is the electron number density. The azimuthal magnetic field B_θ induced by the arc current is evaluated by Maxwell's equation,

$$\frac{1}{r}\frac{\partial}{\partial r}(r B_\theta) = \mu_0 j_z \qquad (8)$$

where μ_0 is the permeability of free space.

The other equations used in this model and detailed boundary conditions are also given in the previous paper[4]. We assumed that the stable argon GTA was instantaneously produced at $\tau = 0$. The τ is the time after arc ignition. Therefore, we do not take into account the phenomena of the arc ignition.

3. Results and Discussion

Figure 2 represents the time dependent two-dimensional distributions of temperature in the whole region of the stationary welding process for a 150 A in DC arc current at 1, 5, 10 and 20 seconds after arc ignition. **Figure 3** also represents the time dependent two-dimensional distributions of fluid flow velocity for the same conditions at the same times after arc ignition. The maximum temperatures of the tungsten cathode and arc plasma are time independently ~3500 K at the tip of the cathode and 17000 K on the arc
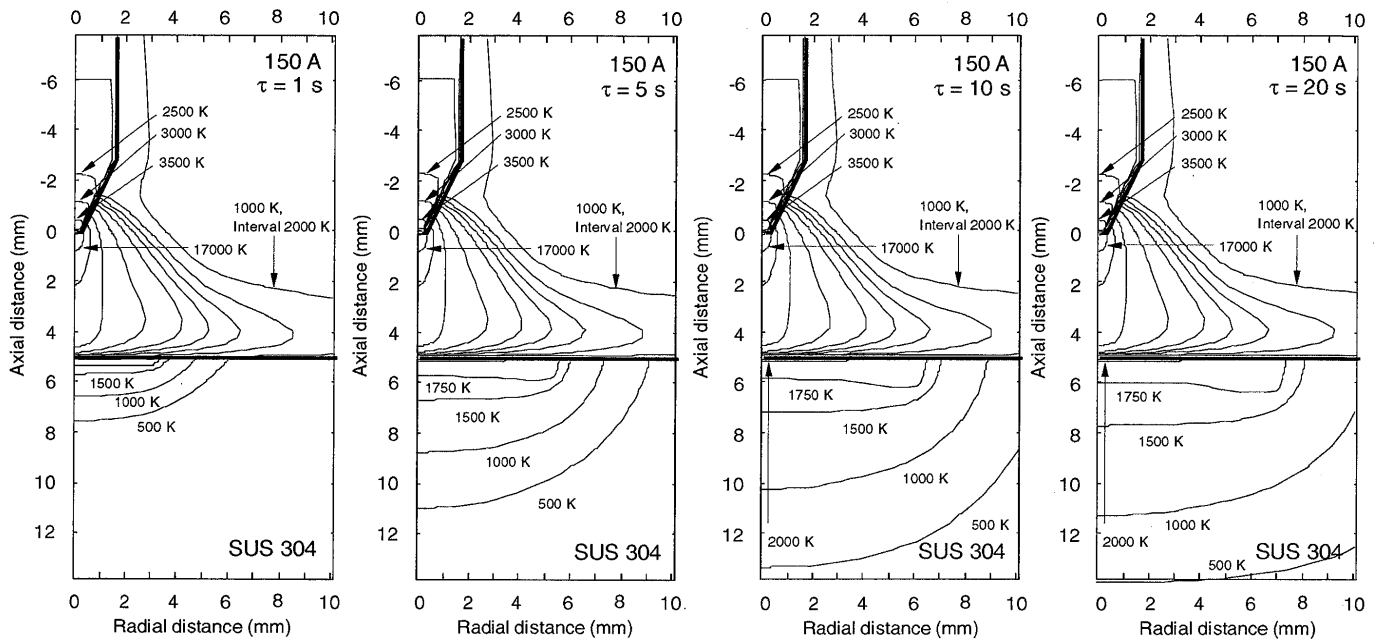
Fig. 2 Predicted time dependent temperature contours for a 150 A in a stationary welding process with SUS304.
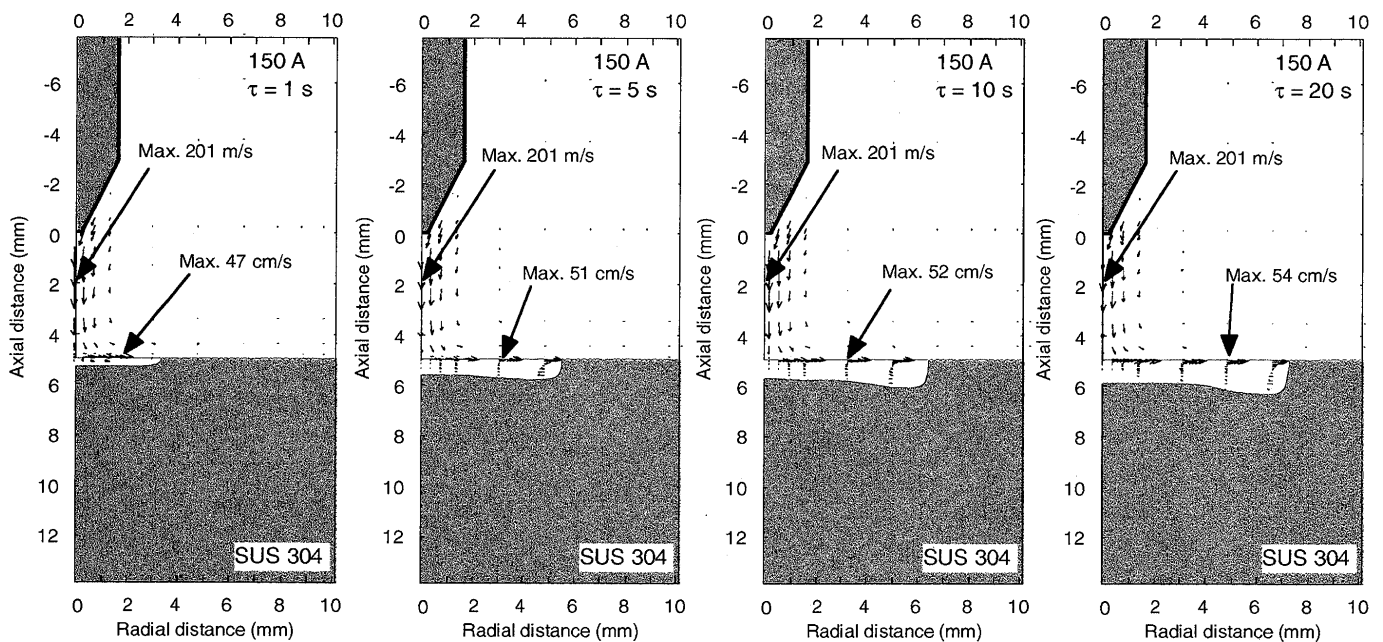

Fig. 3 Predicted time dependent fluid flow velocity for a 150 A in a stationary welding process with SUS304.

axis close to the cathode tip. These predicted maximum temperatures, as well as the other temperatures, are in good agreement with the cathode surface temperatures and ion temperatures measured by Zhou[6] and Tanaka[7], respectively. The weld penetration increases with the elapse of time, and the maximum temperature of the anode becomes 2000 K at the center of the molten anode surface at 20s after arc ignition. The interaction of the arc current with its own magnetic field leads to the phenomena of induced strong mass flow from the cathode to the anode. This induced mass flow is generally called the cathode jet[8]. The maximum

calculated velocity of the cathode jet in Fig. 3 reaches 201 m s^{-1} uniformly for any time. Snyder showed an experimental result of axial velocity in free-burning argon arc by using the laser scattering measurement[9]. His result showed that the cathode jet velocity reached around 300 m s^{-1} for 200 A in arc current. In the case of 150 A in arc current, 100 m s^{-1} ~ 200 m s^{-1} in the cathode jet velocity was reported[10]. Therefore, our calculated result for the cathode jet velocity is in good agreement with the experimental results. This axial fluid flow of the cathode jet changes its direction in front of the anode surface, and then its radial component of
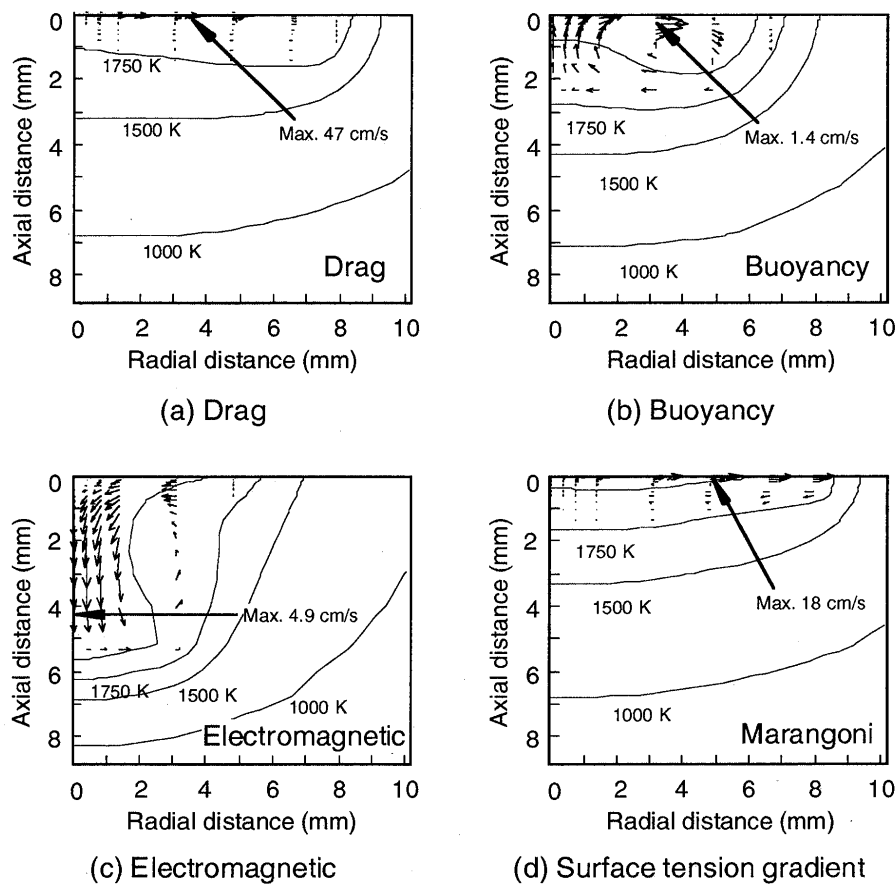
Fig. 4 Temperatures and fluid flow velocities in the welds for individual driving forces corresponding to Fig. 5.
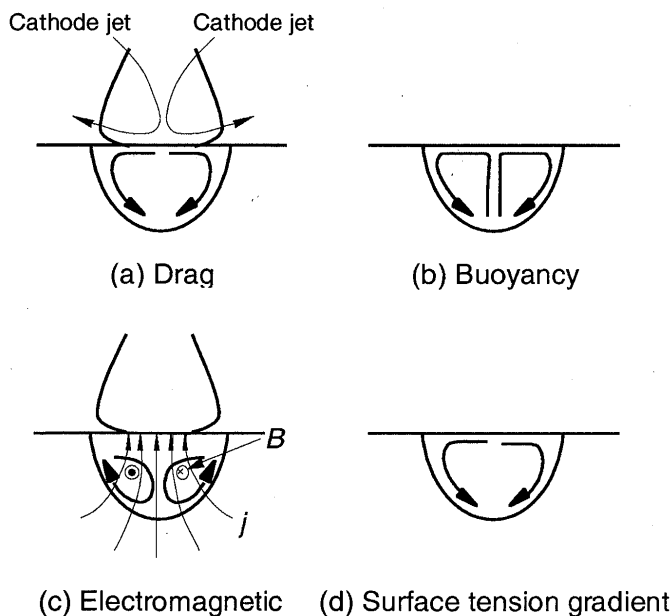

Fig. 5 Flow directions induced by four possible driving forces in the weld pool by GTA welding process.

the fluid flow drags the surface of the weld pool. This drag force is one of the driving forces of outward fluid flow in the weld pool. The outward fluid flow is also caused by the negative temperature coefficient of surface tension assumed in Fig. 1. **Figure 4** shows distributions of temperature and fluid flow velocity of the weld for the individual driving forces corresponding to **Fig. 5**. Figure 5 shows the convective flow directions induced by four possible driving forces in the weld pool, namely, (a) the drag force of the cathode jet, (b) the buoyancy force, (c) the electromagnetic force due to the self-magnetic field of the welding current and (d) the surface tension gradient force which is called the Marangoni force. These calculations were made in the steady state under the same conditions with Figs. 2 and 3. Each maximum velocity for drag, buoyancy, electromagnetic and Marangoni force is 47 cm s^{-1}, 1.4 cm s^{-1}, 4.9 cm s^{-1} and 18 cm s^{-1}, respectively. Figure 4 suggests that the calculated convective flow in the molten anode is dominated by the drag force of the cathode jet and the Marangoni force as compared with the other two driving forces. It also suggests that a balance between the drag force and the Marangoni force should determine the direction of re-circulatory flow in the molten anode. Figure 3 represents a numerical result
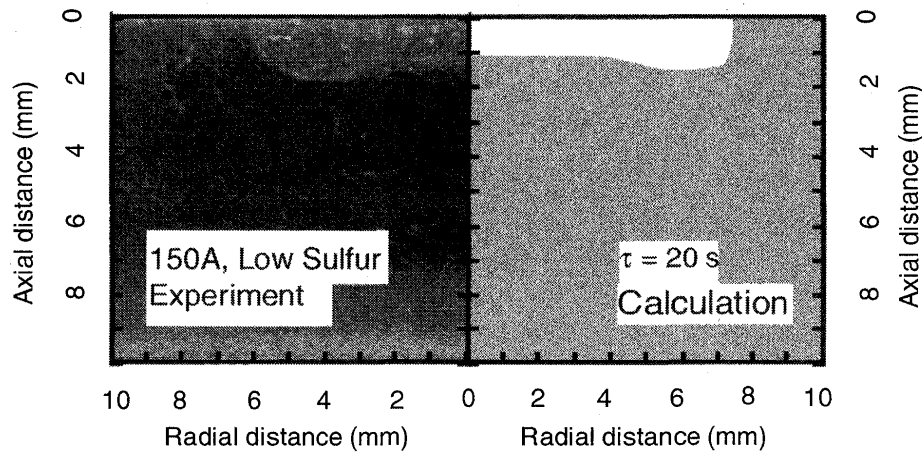
Fig. 6 Comparison of experimental and theoretical weld profiles from 150 A after 20s of arcing.

corresponding to outward fluid flow with a wide and shallow weld penetration which is caused by both outward forces of the drag force and the Marangoni force with the negative temperature coefficient of surface tension. This weld penetration geometry is a typical one in the argon GTA welding process. The maximum calculated velocity in the weld pool for all considered cases reaches 54 cm s⁻¹ at 20s after arc ignition.

Figure 6 shows the predicted weld penetration profile after 20 seconds, compared with an experimental result. The experimental result was taken after 20s of arcing for the same conditions as the calculation. The anode was a disk, 50 mm in diameter and 10 mm in thickness, of SUS 304, mounted into a water-cooled copper plate. We consider that the agreement between the theoretical prediction and the experimental weld profile of Fig. 6 is very good, considering that there is sure to be difference between the value of surface tension as a function of temperature of the experiment and the idealized linear relationship with temperature of Fig. 1 used in the theoretical prediction. Furthermore, differences will also exist between the other physical properties of thermal conductivity, specific heat, and viscosity taken from the literature[11-13] and those occurring in the experiment.

4. Conclusions

1) The whole region of argon GTA welding process, namely, tungsten cathode, arc plasma and weld pool has been treated in a unified numerical model.

2) The time dependent two-dimensional distributions of temperature and velocity were predicted, together with the weld penetration as function of time for a 150 A arc in argon.

3) It was shown that calculated convective flow in the weld pool was mainly dominated by the drag force of the cathode jet and the Marangoni force as compared with the other two driving forces, namely, the buoyancy force and the electromagnetic force. It was suggested that a balance between the drag force and the Marangoni force should determine the direction of re-circulatory flow in the weld pool and then the weld penetration geometry.

References
1) M. Tanaka, T. Shimizu, H. Terasaki, M. Ushio, F. Koshi-ishi and C. L. Yang: Science and Technology of Welding and Joining, 5 (2000), pp.397-402.
2) M. Tanaka, H. Terasaki and M. Ushio: ISIJ Int., 42 (2002), pp.1005-1009.
3) A. Matsunawa: Proceedings of the 3rd International Conference on Trends in Welding Research, Gatlinburg, Tennessee, USA, June 1-5, 1992.
4) M. Tanaka, H. Terasaki, M. Ushio and J.J. Lowke: Metall. Trans. A, 33A (2002), pp.2043-2052.
5) M. Tanaka, M. Ushio and C. S. Wu: J. Phys. D: Appl. Phys. 32 (1999), pp.605-611.
6) X. Zhou and J. Heberlein: J. Phys. D: Appl. Phys. 31 (1998), pp.2577-2590.
7) M. Tanaka and M. Ushio: J. Phys. D: Appl. Phys. 32 (1999), pp.1153-1162.
8) K. C. Hsu, and E. Pfender: J. Appl. Phys., 54 (1983) 4359.
9) S.C. Snyder and R.E. Bentley: J. Phys. D: Appl. Phys. 29 (1996), pp.3045-3049.
10) J.F. Lancaster: The Physics of Welding, Pergamon Press, Oxford (1984).
11) J. F. Elliott and M. Gleiser: Thermochemistry for Steelmaking, Vol. 1, Addison-Wesley (1960).
12) The Japan Inst. Metals: Data-book for Metals, Maruzen, Tokyo (1984) (in Japanese).
13) Japan Stainless Steel Association: Handbook of stainless steel, The Nikkan Kogyo Shimbun, Tokyo (1995) (in Japanese).